



SUSY fits with full LHC Run I data

Kees Jan de Vries (on behalf of the MasterCode Collaboration)^a

^aHigh Energy Physics Group, Blackett Laboratory, Imperial College, Prince Consort Road, London SW7 2AZ, UK

Abstract

We present the latest results from the MasterCode collaboration on supersymmetric models, in particular on the CMSSM, the NUHM1, the NUHM2 and the pMSSM. We combine the data from LHC Run I with astrophysical observables, flavor and electroweak precision observables. We determine the best fit regions of these models and analyze the discovery potential of squarks and gluinos at LHC Run II and direct detection experiments.

Keywords: Supersymmetry, CMSSM, NUHM1, NUHM2, pMSSM

1. Introduction

Despite the absence of any convincing signal of supersymmetry (SUSY) after Run 1 at the large hadron collider (LHC), SUSY remains well motivated. First of all, the lightest neutralino is a natural DM candidate. Secondly, SUSY provides a solution to the hierarchy problem. Finally, SUSY allows for unification of the gauge coupling at the so-called grand unified theory (GUT) scale of $O(10^{16})$ GeV.

In these proceedings we present a selection of the results from global frequentist fits of constrained models of SUSY - the CMSSM, NUHM1, NUHM2 and pMSSM10 (defined below) - to experimental constraints from Run I LHC data, astrophysical observables, flavor and electroweak observables. The fits allow us to identify the relevant parameters, assess and compare the validity of the models and study the predictions and consequences for future searches and experiments. In particular, we focus on the differences between GUT-scale and phenomenological models highlighting the $(g-2)_\mu$ constraint. We discuss the discovery potential for gluinos and squarks at LHC Run II as well as prospects for direct detection of dark matter.

Note that the results presented in these proceedings date from the ICHEP2014 conference. We have published elsewhere some of the results shown in these proceedings, namely on the CMSSM, NUHM1 and

NUHM2 [1, 2]. We would also like to mention that there are several other groups that perform global fits of SUSY using Bayesian as well as frequentist methods. Some recent fits of CMSSM, NUHM1 and NUHM2 may be found in [3–6], whereas results on the pMSSM may be found in [7, 8]. We will soon publish updated results on pMSSM10.

2. Analysis procedure

2.1. Models

We consider four constrained versions of the general R -parity-conserving Minimal Supersymmetric extension of the Standard Model (MSSM). Three of these models are derived from GUT model-building considerations, where masses and couplings are assumed to unify at the GUT scale: In the constrained MSSM (CMSSM) all scalars (two Higgs doublets and the sfermions) have a universal soft SUSY-breaking mass m_0 , the gauginos a universal mass $m_{1/2}$, and the trilinear couplings are all equal to A_0 . In the NUHM1 the masses of the Higgs doublets are assumed to be independent but equal, while in the NUHM2 they are allowed to vary independently. In general m_0^2 can take negative values, and so we denote in this paper $m_0 \equiv \text{Sign}(m_0^2) \sqrt{|m_0^2|} < 0$. The remaining parameters of these models are the superpotential coupling μ between the Higgs doublets

and the ratio of the vacuum expectation values of the two Higgs doublets, $\tan\beta \equiv v_1/v_2$. We also consider a 10-dimensional subset of the so-called phenomenological MSSM (pMSSM)[9], which makes no assumptions about the masses at the GUT-scale. Instead in the pMSSM the soft SUSY-breaking parameters are defined at the SUSY-breaking scale $M_{SUSY} \sim \sqrt{m_{\tilde{t}_1} \cdot m_{\tilde{t}_2}}$. It also is assumed there are no flavor-changing neutral currents, no additional sources of CP violation as well as unification of the first and second generation sfermion masses. Our 10-dimensional subset of the pMSSM (pMSSM10) is defined as follows. We set all first and second generation squark masses to a common value $m_{\tilde{q}_{12}}$, all third-generation squark mass parameters to a common value $m_{\tilde{q}_3}$, the slepton masses to $m_{\tilde{l}}$, and the trilinear couplings $A_t = A_b = A_\tau = A$. The remaining parameters are the gaugino masses, M_1, M_2, M_3 , the Higgs mixing parameter μ , the CP-odd Higgs mass scale M_A , and $\tan\beta$.

2.2. Fitting procedure

We construct a χ^2 function in the same way as in [2, 10], taking into account constraints from B-physics, electroweak precision observables, cosmology and direct SUSY searches at the LHC. The only difference of the χ^2 function between the models is the way we implement the direct SUSY searches. For the CMSSM, NUHM1 and NUHM2 we use the latest results from the jets + E_T analysis of ATLAS [11] and apply the constraint as we previously described in [1]. For the pMSSM10 we use a 4-dimensional lookup table in $(m_{\tilde{\chi}^0}, m_{\tilde{g}}, m_{\tilde{q}_{12}}, m_{\tilde{q}_3})$. The underlying principle of this method is that, to good approximation, the limits from direct SUSY searches are independent of the configuration of the sleptons and the other gauginos as was argued in [12]. We use the same framework as was used for that work, using 7 TeV searches of CMS [13–16]. We have extensively validated this approach but details are beyond the scope of these proceedings, and will be presented in future work.

Finally, we use the MasterCode framework to calculate the observables that go into the χ^2 calculation. The MasterCode framework interfaces various public and private codes using the SLHA format [17]. In particular we use SOFTSUSY [18] to calculate the spectra, FeynHiggs [19] to calculate Higgs observables and $(g-2)_\mu$, MicrOMEGAS [20] to calculate the relic DM density, SuFla [21, 22] for B-physics observables, FeynWZ [23, 24] for EWPOs, and SSARD for the spin-independent cross section. We use the Multinest package [25] for sampling.

3. Results

3.1. $(m_0, m_{1/2})$ plane of the CMSSM, NUHM1 and NUHM2

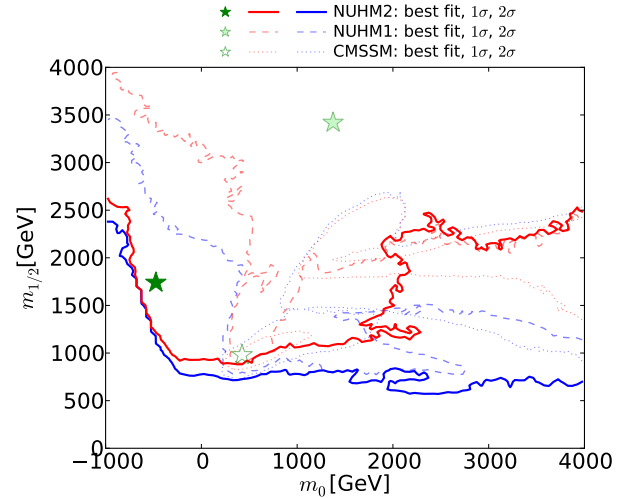


Figure 1: The $(m_0, m_{1/2})$ parameter plane of the CMSSM, NUHM1 and NUHM2. Red (blue) dotted, dashed and solid contours correspond to their respective 68% (95%) CL, whereas empty, shaded green and filled stars correspond to their respective best fit points.

Let us first turn to the $(m_0, m_{1/2})$ parameter plane of the CMSSM, NUHM1 and NUHM2 in Fig. 1. In this figure the red (blue) dotted, dashed, and solid lines correspond to the 68% (95%) CL contours of the CMSSM, NUHM1 and NUHM2 respectively. The empty, light shaded green and green filled stars denote the respective best fit points.

In the CMSSM there appears a bimodal structure, with one local minimum around $m_0 \sim 400$ and $m_{1/2} \sim 1000$ GeV and another that stretches to high values of m_0 at high $m_{1/2}$. These modes correspond to two different mechanisms to fulfil the relic DM density constraint, namely stau coannihilation and the heavy Higgs (H/A) funnel respectively. We see that in the displayed region of the CMSSM, the $m_{1/2}$ parameter has an upper bound of approximately 2.5 TeV, it should be stressed that this lower bound increases for larger values of m_0 . The lower bound on $m_{1/2}$ at $m_0 \sim 2$ TeV is mainly due to the $\text{BR}(B_s \rightarrow \mu^+ \mu^-)$ constraint. From our previous fits [1, 26] we know that the $(g-2)_\mu$ constraint prefers low values of m_0 and $m_{1/2}$, which are in tension with the absence of any signal from searches for SUSY particles at the LHC.

In the NUHM1 we note that there is no longer an upper bound on $m_{1/2}$. The region that has become avail-

able at $m_{1/2} \gtrsim 2.5$ TeV is characterized by chargino coannihilation. We also see that in the NUHM1 negative values of m_0 are accessible at $m_{1/2} \gtrsim 2.2$ TeV at 95% CL. In this region both stau and chargino coannihilation are responsible for fulfilling the relic DM density constraint. Stau coannihilation and the H/A funnel appear at similar places as in the CMSSM. In the NUHM2, the extra degree of freedom allows the stau coannihilation region to expand to negative values of m_0 at low values of $m_{1/2}$.

We would like to emphasize that in general the 68% and 95% CL contours extend beyond the boundary of the sampled parameter ranges. This highlights the fact that the minimum structure is very shallow and there is no particularly favored region in the parameter space.

3.2. The anomalous magnetic dipole moment of the muon $(g-2)_\mu$

There is a discrepancy of $\sim 3.5\sigma$ between the measurement [27] and the theoretical SM calculation [28] (and references therein) of the $(g-2)_\mu$. This discrepancy can be interpreted as arising from SUSY contributions, see e.g. [29]. Sizable SUSY contributions can arise when neutralinos, charginos, smuons and muon sneutrinos have masses of $\mathcal{O}(100$ GeV). However, one has to keep in mind that in GUT-models the chargino and neutralino masses are directly proportional to the gluino mass, and are hence directly constrained by gluino searches at the LHC. Similarly, the smuon and muon sneutrino masses are constrained by searches for colored sparticles at the LHC. These searches have in general a greater sensitivity than searches for electroweakly interacting sparticles.

In global fits of the CMSSM and NUHM1[1] we found that indeed $(g-2)_\mu$ cannot be reconciled with the non-observation of sparticles at the LHC. The question is whether the additional freedom in NUHM2 and pMSSM10 allows for $(g-2)_\mu$ to be fulfilled. Fig. 2 displays the total χ^2 as a function of half the difference between the predicted value of $(g-2)_\mu$ and the SM value $\Delta\left(\frac{g-2}{2}\right)$ for the CMSSM, NUHM1, NUHM2 and pMSSM10 in dotted blue, dashed blue, solid blue and solid black respectively. To guide the eye a green vertical line is displayed to indicate where $(g-2)_\mu$ equals the SM value. A shaded red band indicates the current experimental value.

We see that in the CMSSM and NUHM1 $(g-2)_\mu$ cannot be fulfilled. Other constraints, in particular ATLAS jets + E_T search, force $(g-2)_\mu$ to take values close to the SM prediction. In the NUHM2, however, we see that we can indeed get $(g-2)_\mu$ at the measured value,

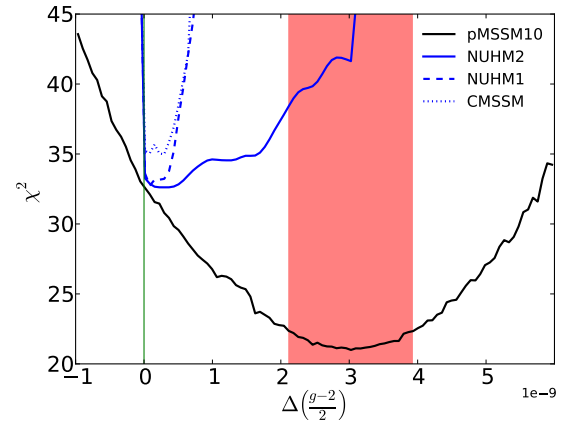


Figure 2: Total χ^2 distribution for SUSY contribution to the anomalous magnetic dipole moment of the muon $\Delta\left(\frac{g-2}{2}\right)$. The green line corresponds to the SM value, whereas the red band corresponds to the measured value and its uncertainty.

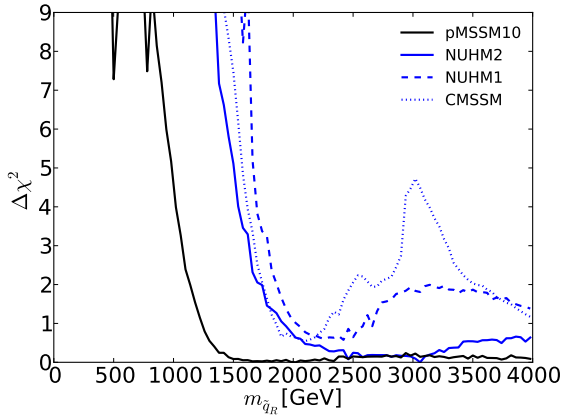
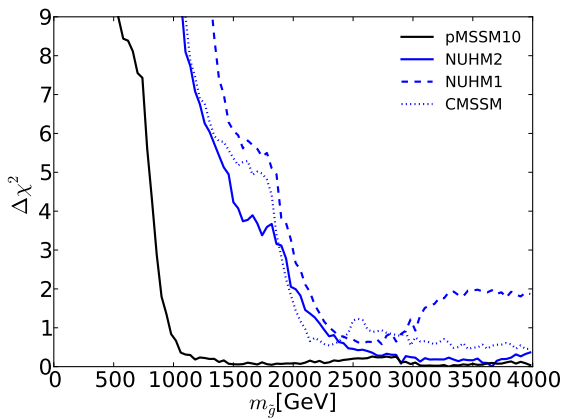
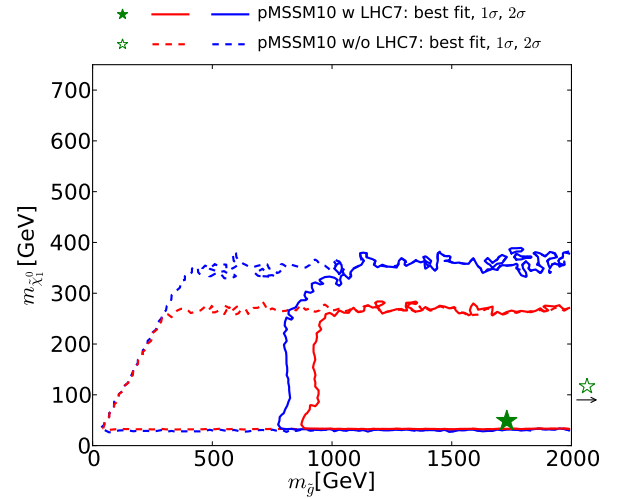
although at the expense of other constraints, notably M_h and the ATLAS constraint. In the pMSSM10 the tension is completely lifted.

Table 1 shows the total χ^2 over the number of degrees of freedom and the corresponding p -values for the CMSSM, NUHM1, NUHM2 and pMSSM10. We note that the total χ^2 drops by more than 10 units when going from the NUHM2 to the pMSSM10. Correspondingly, the p -value increases from $\sim 5.2\%$ to $\sim 21\%$ indicating a significant improvement of the fit. From Fig. 2 it is obvious that the greatest improvement is gained from reconciling the SUSY interpretation of $(g-2)_\mu$ with the other constraints. Hence, the pMSSM10 does indeed allow the tension between $(g-2)_\mu$ and other constraints to be lifted.

3.3. LHC Run 2 discovery potential of squarks and gluinos

We now turn to the one-dimensional profile likelihoods for the right-handed first- and second-generation squark and gluino masses in Fig. 3 and Fig. 4 respectively. In these figures the CMSSM, NUHM1, NUHM2 and pMSSM10 results are indicated by dotted blue, dashed blue, solid blue and solid black respectively. We first observe that lower bounds on the gluino and the squark masses in the CMSSM, NUHM1 and NUHM2 are almost identical, namely ~ 1.7 TeV for the right handed squarks and ~ 1.8 TeV for the gluinos at $\Delta\chi^2 \sim 4$. In the CMSSM the bimodal structure is again visible for the squark mass. To a lesser extent this is true for the NUHM1 and NUHM2. The lower bounds in the

Model	$\chi^2/\text{d.o.f.}$	p -value
CMSSM	35.0/23	5.2 %
NUHM1	32.7/22	6.6 %
NUHM2	32.5/21	5.2 %
pMSSM10	21.3/17	21 %

Table 1: Minimum values of the total χ^2 over the number of degrees of freedom and the corresponding p -value for each model model.Figure 3: $\Delta\chi^2$ distribution for the first and second generation (right-handed) squark masses. The blue dotted, blue dashed, blue solid and black solid lines correspond to CMSSM, NUHM1, NUHM2 and pMSSM10 respectively. Note that the pMSSM10 results are only for LHC7 data.Figure 4: $\Delta\chi^2$ distribution for the gluino mass. The blue dotted, blue dashed, blue solid and black solid lines correspond to CMSSM, NUHM1, NUHM2 and pMSSM10 respectively. Note that the pMSSM10 results are only for LHC7 data.Figure 5: The $(m_{\tilde{g}}, m_{\tilde{\chi}_1^0})$ plane in the pMSSM10, with and without the colored searches at 7 TeV (indicated as LHC7) applied. The red (blue) solid and dashed contours correspond to 68% (95%) CL respectively, whereas the filled and empty star correspond to the respective best fit points. Note that the best fit point without LHC7 applied lies outside the plotted range. An arrow indicates its position.

pMSSM10 are significantly lower, which is expected because only the 7 TeV limits have been applied.

The predictions for the squarks and gluinos may be compared (with some caveats) to a study by the ATLAS collaboration [30], Fig. 5(a). According to this figure, the exclusion potential after 300 fb^{-1} at 14 TeV is $\sim 2.7 \text{ TeV}$ ($\sim 2.3 \text{ TeV}$) for $m_{\tilde{q}}$ ($m_{\tilde{g}}$), irrespective of $m_{\tilde{g}}(m_{\tilde{q}})$, when assuming $m_{\tilde{\chi}_1^0} = 0 \text{ GeV}$. According to these numbers, the lower-mass mode of the CMSSM should be accessible in LHC Run II. However, masses higher than $\sim 3 \text{ TeV}$ might be beyond reach even at high luminosity LHC.

In Fig. 5 we display the $(m_{\tilde{g}}, m_{\tilde{\chi}_1^0})$ plane for the pMSSM10. In this figure the solid and dashed red (blue) contours correspond to 68% (95%) CL of the pMSSM10 with and without the LHC searches for sparticles applied respectively. The filled and the empty star correspond to their respective best-fit points. A very

important feature is that in the pMSSM10 the gluino and neutralino mass are completely independent, as opposed to GUT-scale models which have a fixed relationship between these masses. This freedom corresponds nicely to possibilities studied by the CMS and ATLAS experiments in simplified models [31]. We also see that values $m_{\tilde{\chi}_1^0} \lesssim 300$ are preferred. This strong preference can be understood from the fulfillment of the $(g-2)_\mu$ constraint. The gluino mass is generally unconstrained once it is above the CMS-imposed lower bound.

3.4. Direct Dark Matter detection

Finally we turn to predictions for the spin-independent cross-section as a function of the lightest neutralino mass in Fig. 6. Here we overlaid our results on the summary plot of the Snowmass CF1 Summary [32]. The summary plot shows current upper bounds on the spin-independent cross section as a function of the lightest neutralino mass from various experiments using solid lines. Dashed lines indicate the projected sensitivity of future searches. The yellow region indicates where backgrounds from solar and atmospheric neutrinos dominate over the DM signal. We will refer to this boundary as the neutrino floor. Our results are shown in solid, dashed-dotted, dashed and dotted red (blue) contours corresponding to 68% and (95%) CL for the pMSSM10, NUHM2, NUHM1 and CMSSM respectively. The black, green, light shaded green and empty stars correspond to their best fit points respectively.

We see that future experiments would probe a significant part of the parameter space of the CMSSM, and all of the preferred regions are above the neutrino floor. For the NUHM1 some of the allowed region is below the neutrino floor, whereas the NUHM2 even has its best-fit point in this region. In the pMSSM10, the preferred masses of the lightest neutralino are significantly lower than those in the CMSSM, NUHM1 or NUHM2. Another striking feature of the pMSSM10 is that the cross sections can go down to the extremely low value of $\sigma_p^{SI} \ll 10^{-50}$, which would make it very hard if not impossible for direct detection experiments to measure dark matter scattering.

4. Conclusion

In supergravity-inspired models like the CMSSM, NUHM1 and NUHM2, there has been an ever growing tension between a supersymmetric interpretation of $(g-2)_\mu$ and the searches for SUSY particles and other new phenomena at the LHC during Run 1. We showed that even the extra freedom in the NUHM2 cannot resolve this tension. However, in the pMSSM10, where

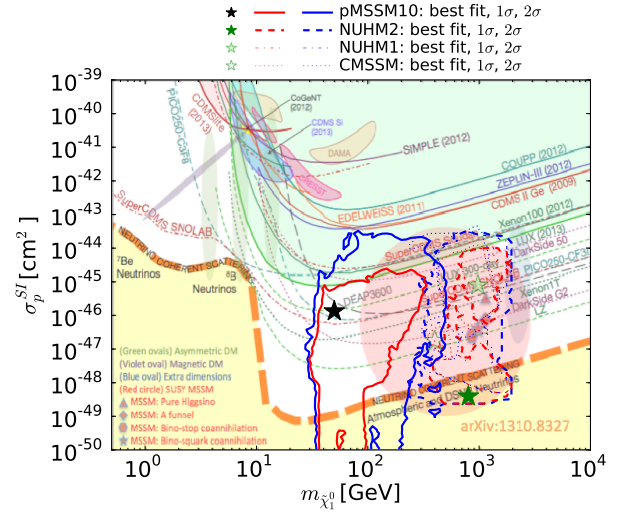


Figure 6: Our results for $(m_{\tilde{\chi}_1^0}, \sigma_p^{SI})$ plane of the CMSSM, NUHM1, NUHM2 and pMSSM10 overlaid on the summary plot from Snowmass CF1 Summary [32]. The description of the summary plot can be found in the text. The overlaid red (blue) dotted, dashed-dotted, dashed and solid correspond to the 68% (95%) CL for the CMSSM, NUHM1, NUHM2 and pMSSM10 respectively, whereas the empty, shaded green, green filled and black stars correspond to their best fit points.

no GUT-scale unifying assumptions are made, it is indeed possible to reconcile $(g-2)_\mu$ with the measurements and non-measurements at the LHC. This significantly improves the fit. In particular, the p -value increases from $\sim 5\%$ to $\sim 20\%$ when going from the SUGRA models to pMSSM10.

We discussed the discovery potential of the first two generations (right-handed) squarks and gluinos at LHC Run II. The CMSSM, NUHM1 and NUHM2 have very similar lower limits of ~ 1.7 TeV for the squarks and ~ 1.8 TeV for the gluinos. The lower bounds for the pMSSM10 are lower, but one has to keep in mind that we only applied 7 TeV limits. Comparing to predicted sensitivities from ATLAS [30], it seems that the mode at low mass in the CMSSM will be within reach of LHC Run II. The other models also have good parameter space within reach. However, the gluino and squark masses are generally unconstrained when above the ATLAS/CMS-imposed lower bounds. Nevertheless, the pMSSM10 already provides complementary information compared to GUT models, as the relations between the gluino and neutralinos are completely lifted.

Finally we saw that future dark matter direct detection experiments will have access to a significant part of the parameter space of the CMSSM, NUHM1 and

NUHM2. However some of the preferred regions for the latter two lie in the region where the background from atmospheric neutrinos dominates. In the pMSSM10, very low spin-independent cross sections are possible. Scattering cross-sections below the neutrino floor might render it very hard if not impossible for direct detection experiments to measure any signal.

References

- [1] O. Buchmueller, R. Cavanaugh, A. De Roeck, M. Dolan, J. Ellis, et al., The CMSSM and NUHM1 after LHC Run 1, *Eur.Phys.J. C74* (2013) 2922. [arXiv:1312.5250](#), [doi:10.1140/epjc/s10052-014-2922-3](#).
- [2] O. Buchmueller, R. Cavanaugh, M. Citron, A. De Roeck, M. Dolan, et al., The NUHM2 after LHC Run 1 [arXiv:1408.4060](#).
- [3] P. Bechtle, T. Bringmann, K. Desch, H. Dreiner, M. Hamer, et al., Constrained Supersymmetry after two years of LHC data: a global view with Fittino, *JHEP* 1206 (2012) 098. [arXiv:1204.4199](#), [doi:10.1007/JHEP06\(2012\)098](#).
- [4] P. Scott, et al., Use of event-level neutrino telescope data in global fits for theories of new physics, *JCAP* 1211 (2012) 057. [arXiv:1207.0810](#), [doi:10.1088/1475-7516/2012/11/057](#).
- [5] C. Stenge, G. Bertone, F. Feroz, M. Fornasa, R. Ruiz de Austri, et al., Global Fits of the cMSSM and NUHM including the LHC Higgs discovery and new XENON100 constraints, *JCAP* 1304 (2013) 013. [arXiv:1212.2636](#), [doi:10.1088/1475-7516/2013/04/013](#).
- [6] L. Roszkowski, E. M. Sessolo, A. J. Williams, What next for the CMSSM and the NUHM: Improved prospects for superpartner and dark matter detection, *JHEP* 1408 (2014) 067. [arXiv:1405.4289](#), [doi:10.1007/JHEP08\(2014\)067](#).
- [7] C. Boehm, P. S. B. Dev, A. Mazumdar, E. Pukartas, Naturalness of Light Neutralino Dark Matter in pMSSM after LHC, XENON100 and Planck Data, *JHEP* 1306 (2013) 113. [arXiv:1303.5386](#), [doi:10.1007/JHEP06\(2013\)113](#).
- [8] C. Stenge, G. Bertone, G. Besjes, S. Caron, R. Ruiz de Austri, et al., Profile likelihood maps of a 15-dimensional MSSM, *JHEP* 1409 (2014) 081. [arXiv:1405.0622](#), [doi:10.1007/JHEP09\(2014\)081](#).
- [9] A. Djouadi, et al., The Minimal supersymmetric standard model: Group summary report [arXiv:hep-ph/9901246](#).
- [10] F. Feroz, K. Cranmer, M. Hobson, R. Ruiz de Austri, R. Trotta, Challenges of Profile Likelihood Evaluation in Multi-Dimensional SUSY Scans, *JHEP* 1106 (2011) 042. [arXiv:1101.3296](#), [doi:10.1007/JHEP06\(2011\)042](#).
- [11] G. Aad, et al., Search for squarks and gluinos with the ATLAS detector in final states with jets and missing transverse momentum using $\sqrt{s} = 8$ TeV proton–proton collision data, *JHEP* 1409 (2014) 176. [arXiv:1405.7875](#), [doi:10.1007/JHEP09\(2014\)176](#).
- [12] O. Buchmueller, J. Marrouche, Universal mass limits on gluino and third-generation squarks in the context of Natural-like SUSY spectra, *Int.J.Mod.Phys. A29* (2014) 1450032. [arXiv:1304.2185](#), [doi:10.1142/S0217751X14500328](#).
- [13] S. Chatrchyan, et al., Search for supersymmetry in final states with missing transverse energy and 0, 1, 2, or at least 3 b-quark jets in 7 TeV pp collisions using the variable α_T , *JHEP* 1301 (2013) 077. [arXiv:1210.8115](#), [doi:10.1007/JHEP01\(2013\)077](#).
- [14] S. Chatrchyan, et al., Search for supersymmetry in pp collisions at $\sqrt{s} = 7$ TeV in events with a single lepton, jets, and missing transverse momentum, *Eur.Phys.J. C73* (2013) 2404. [arXiv:1212.6428](#), [doi:10.1140/epjc/s10052-013-2404-z](#).
- [15] S. Chatrchyan, et al., Search for new physics in events with opposite-sign leptons, jets, and missing transverse energy in pp collisions at $\sqrt{s} = 7$ TeV, *Phys.Lett. B718* (2013) 815–840. [arXiv:1206.3949](#), [doi:10.1016/j.physletb.2012.11.036](#).
- [16] S. Chatrchyan, et al., Search for new physics in events with same-sign dileptons and b -tagged jets in pp collisions at $\sqrt{s} = 7$ TeV, *JHEP* 1208 (2012) 110. [arXiv:1205.3933](#), [doi:10.1007/JHEP08\(2012\)110](#).
- [17] B. Allanach, C. Balazs, G. Belanger, M. Bernhardt, F. Boudjema, et al., SUSY Les Houches Accord 2, *Comput.Phys.Commun.* 180 (2009) 8–25. [arXiv:0801.0045](#), [doi:10.1016/j.cpc.2008.08.004](#).
- [18] B. Allanach, SOFTSUSY: a program for calculating supersymmetric spectra, *Comput.Phys.Commun.* 143 (2002) 305–331. [arXiv:hep-ph/0104145](#), [doi:10.1016/S0010-4655\(01\)00460-X](#).
- [19] T. Hahn, S. Heinemeyer, W. Hollik, H. Rzehak, G. Weiglein, High-precision predictions for the light CP-even Higgs Boson Mass of the MSSM, *Phys.Rev.Lett.* 112 (2014) 141801. [arXiv:1312.4937](#), [doi:10.1103/PhysRevLett.112.141801](#).
- [20] G. Belanger, F. Boudjema, A. Pukhov, A. Semenov, micrOMEGAs.3: A program for calculating dark matter observables, *Comput.Phys.Commun.* 185 (2014) 960–985. [arXiv:1305.0237](#), [doi:10.1016/j.cpc.2013.10.016](#).
- [21] G. Isidori, P. Paradisi, Hints of large $\tan(\beta)$ in flavour physics, *Phys.Lett. B639* (2006) 499–507. [arXiv:hep-ph/0605012](#), [doi:10.1016/j.physletb.2006.06.071](#).
- [22] G. Isidori, F. Mescia, P. Paradisi, D. Temes, Flavour physics at large $\tan(\beta)$ with a Bino-like LSP, *Phys.Rev. D75* (2007) 115019. [arXiv:hep-ph/0703035](#), [doi:10.1103/PhysRevD.75.115019](#).
- [23] S. Heinemeyer, W. Hollik, D. Stockinger, A. Weber, G. Weiglein, Precise prediction for $M(W)$ in the MSSM, *JHEP* 0608 (2006) 052. [arXiv:hep-ph/0604147](#), [doi:10.1088/1126-6708/2006/08/052](#).
- [24] S. Heinemeyer, W. Hollik, A. Weber, G. Weiglein, Z Pole Observables in the MSSM, *JHEP* 0804 (2008) 039. [arXiv:0710.2972](#), [doi:10.1088/1126-6708/2008/04/039](#).
- [25] F. Feroz, M. Hobson, M. Bridges, MultiNest: an efficient and robust Bayesian inference tool for cosmology and particle physics, *Mon.Not.Roy.Astron.Soc.* 398 (2009) 1601–1614. [arXiv:0809.3437](#), [doi:10.1111/j.1365-2966.2009.14548.x](#).
- [26] O. Buchmueller, R. Cavanaugh, M. Citron, A. De Roeck, M. Dolan, et al., The CMSSM and NUHM1 in Light of 7 TeV LHC, B_s to $\mu+\mu-$ and XENON100 Data, *Eur.Phys.J. C72* (2012) 2243. [arXiv:1207.7315](#), [doi:10.1140/epjc/s10052-012-2243-3](#).
- [27] G. Bennett, et al., Final Report of the Muon E821 Anomalous Magnetic Moment Measurement at BNL, *Phys.Rev. D73* (2006) 072003. [arXiv:hep-ex/0602035](#), [doi:10.1103/PhysRevD.73.072003](#).
- [28] M. Benayoun, P. David, L. DelBuono, F. Jegerlehner, An Update of the HLS Estimate of the Muon $g-2$, *Eur.Phys.J. C73* (2013) 2453. [arXiv:1210.7184](#), [doi:10.1140/epjc/s10052-013-2453-3](#).
- [29] D. Stockinger, The Muon Magnetic Moment and Supersymmetry, *J.Phys. G34* (2007) R45–R92. [arXiv:hep-ph/0609168](#), [doi:10.1088/0954-3899/34/2/R01](#).
- [30] [link].
URL <https://twiki.cern.ch/twiki/bin/view/>

CMSPublic/PhysicsResultsSUS

- [31] D. Alves, et al., Simplified Models for LHC New Physics Searches, *J.Phys. G*39 (2012) 105005. [arXiv:1105.2838](#), [doi:10.1088/0954-3899/39/10/105005](#).
- [32] P. Cushman, C. Galbiati, D. McKinsey, H. Robertson, T. Tait, et al., Working Group Report: WIMP Dark Matter Direct Detection [arXiv:1310.8327](#).